Published in IET Microwaves, Antennas & Propagation
Received on 30th April 2009
Revised on 9th December 2009
doi: 10.1049/iet-map.2009.0232

In Special Issue on Asia-Pacific Microwave Conference

ISSN 1751-8725

Design of a novel ultra-high frequency radio-frequency identification reader antenna for near-field communications using oppositely directed currents

C. Cho[1] *J. Ryoo*[2] *I. Park*[3] *H. Choo*[4]

[1]*Institute of Advanced Technologies, Samsung Thales, Yongin, Korea*
[2]*Communication Research Lab., Central R&D Center, LS Industrial Systems, Kyunggi, Korea*
[3]*Department of Electrical and Computer Engineering, Ajou University, Suwon, Korea*
[4]*School of Electronic and Electrical Engineering, Hongik University, Seoul, Korea*
E-mail: hschoo@hongik.ac.kr

Abstract: The authors propose a novel ultra-high frequency (UHF) near-field reader antenna that produces a strong and uniform magnetic near field over a broad region to detect radio-frequency identification (RFID) tags attached to various target objects consistently. The concept of two closely spaced oppositely directed currents (ODCs) is used to obtain a strong magnetic near field, and a symmetrical inverted-L structure fed by a coaxial feed with a parasitic patch is employed as the antenna body to realise the ODCs without any additional feed network. The design parameters were optimised using the Pareto genetic algorithm (GA) in conjunction with the FEKO EM simulator. The optimised antenna had an average magnetic near field of -20 dBA/m in the reading region ($30 \times 30 \times 10$ cm^3), which is suitable for commercial smart-shelf applications. Finally, we examined the effect on our proposed antenna of placing objects in the reading region. The results show that our antenna is appropriate for smart shelves with item-level tagging.

1 Introduction

Recently, radio-frequency identification (RFID) systems for ultra-high frequency (UHF) near-field communications have been used for item-level tagging, as they can detect tags on various target objects more consistently [1–4]. Near-field UHF RFID systems dramatically increase reading stability, because the RF power of the reader is predominantly delivered to passive tags using the magnetic near field, which passes through dielectric materials with very low signal attenuation [5]. In addition, near-field systems allow considerably smaller tags than those used in far-field systems, broadening the range of applications of RFID to extremely small items [6, 7].

Unlike RFID systems for far-field communications, in near-field RFID systems the reader antenna has to generate a strong magnetic field. For example, identifying a commercial Gen2 micro-chip tag using a 0.5-cm radius loop antenna requires the component of the magnetic field normal to the surface of the antenna, H_z, to be at least -20 dBA/m which is obtained from several measurements and will be confirmed using Ampere's law in the next chapter [8, 9]. In addition H_z should be uniformly distributed to remove nulls in the reading zone and increase reading stability.

Among the various types of antenna, single- or multi-turn loop antennas are the most commonly used in near-field reader antennas, because of their ability to generate a strong magnetic field. However, single- and multi-turn loop antennas often exhibit nulls in H_z when the circumference of the loop is greater than 0.5 λ, decreasing reading stability. On the other hand, loops with a smaller

circumference produce a strong magnetic field at the centre of the loop, but the strength of the magnetic field decreases rapidly with distance from the midpoint, resulting in a limited reading area.

We propose a novel near-field reader antenna for UHF RFID systems. The antenna is based on the principle that two closely spaced, oppositely directed currents (ODCs) generate a strong magnetic field over a broad surface area. In contrast to single- or multi-turn loops, the proposed antenna allows nulls in the magnetic field to be removed easily and the amplitude, length and location of the ODCs to be tuned to obtain a uniformly distributed magnetic near field. The antenna body is a symmetrical inverted-L structure fed by a coaxial feed in combination with a parasitic patch to produce the ODCs. In a $30 \times 30 \times 10\,\text{cm}^3$ reading region, average H_z is about -20 dBA/m. Tests of the proposed antenna in smart-shelf applications demonstrated that it is a feasible near-field reader antenna, with commercial applications.

In Section 2, the use of ODCs to obtain a strong magnetic field is explained. Section 3 describes the implementation and optimisation of the ODC idea using Pareto genetic algorithm (PGA), and Section 4 presents the experimental verification of the optimised results.

2 ODCs for UHF smart shelves

The objective of this study was to design a near-field antenna for smart-shelf applications, based on a surface area of $30 \times 30\,\text{cm}^2$ and a reading distance of at least 10 cm (reading volume $>30 \times 30 \times 10\,\text{cm}^3$). It was assumed that multiple target tags would be placed on the smart shelf simultaneously, and that they would be attached to targets that adversely affect EM propagation (for example, a high dielectric material such as plastic bottles with liquid contents). To improve readability, even under such difficult conditions, near-field reader antennas predominantly deliver the RF power to passive tags using the magnetic near field, H_z (where the z-direction is normal to the antenna surface). Therefore unlike systems designed for far-field communications, a near-field reader antenna can generate a broad, strong and uniform magnetic field. For example, to operate a Gen2 micro-chip with $P_{\text{chip,min}}$ of about -10 dBm [10–12] near a small loop 0.5-cm-radius antenna, H_z must be at least -20 dBA/m. To achieve stable readability, H_z should also have uniform distribution (without nulls) over the surface of the smart shelf.

To satisfy the above specifications, we propose the concept of ODCs, as shown in Fig. 1. Two closely spaced ODCs create a strong magnetic field between them, and by adjusting the amplitude, length and location of each current, the null in H_z can be removed. Fig. 2 shows the near-field H_z distribution for two different spacings, d, between two ODC-carrying conductors. H_z was examined at the surface, which was 10 cm above the current elements. Whereas the single dipole produced a very weak

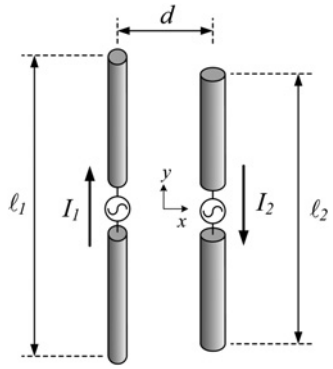

Figure 1 *Concept of ODCs*

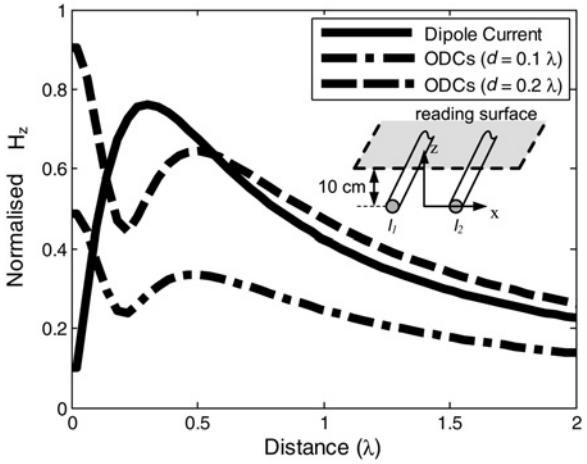

Figure 2 *H_z as a function of the distance between the ODCs*
For comparison, the H_z field distribution of a single half-wavelength dipole is plotted as a solid line

H_z around $x = 0$, that produced by ODCs was much stronger. The H_z distribution was made both more uniform and stronger by adjusting the length of, and current in, each dipole. Fig. 3 shows that H_z was uniformly distributed over the target reading region ($30 \times 30 \times 10\,\text{cm}^3$) when the ODC parameters were: $I_1 = 1$ A, $I_2 = -0.76$ A, $\ell_1 = 0.5\lambda$, $\ell_2 = 0.35\lambda$ and $d = 0.15\lambda$.

This shows that ODCs provide a very effective way of generating a strong and uniform magnetic field in the target reading area, as compared to the use of conventional dipole-type antennas.

ODCs can be realised using a dual feed system, whereby the signal at each dipole is π-phase shifted, as shown in Fig. 1. However, multiple feeds increase the complexity of an antenna system and hence its manufacturing cost. Thus, we realised the ODCs in a single-feed system, by coupling the main wire and the nearby parasitic wire. As shown in Fig. 4, the phase of the current induced in the parasitic wire changes with the distance, d, between the parasitic and main wires. The current phase in the parasitic wire can be

doi: 10.1049/iet-map.2009.0232

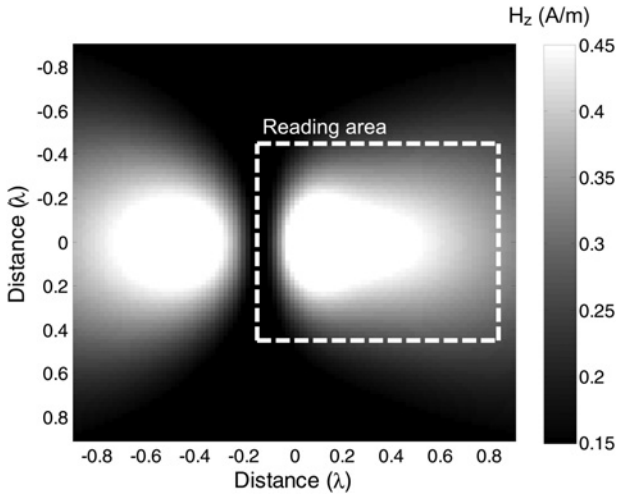

Figure 3 *H_z distribution over the reading area*

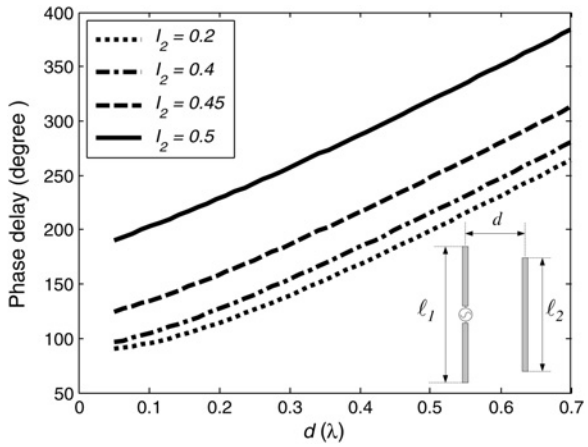

Figure 4 *Phase current delay in the parasitic wire*

calculated using the induced electromotive force. If the radius of each wire, ρ, is assumed to be small, then the self-impedance of each wire (Z_{11}, Z_{22}) is calculated from [13, 14]

$$Z_{mn} = \frac{j\eta_0}{4\pi} \frac{1}{\sin(\beta\ell_m/2)\sin(\beta\ell_n/2)} \int_{-\ell_m/2}^{\ell_m/2} \left[\left(\frac{e^{-j\beta R_1}}{R_1} + \frac{e^{-j\beta R_2}}{R_2} - 2\cos\left(\frac{\beta\ell_n}{2}\right)\frac{e^{-j\beta R_0}}{R_0} \right) \times \sin\beta\left(\frac{\ell_m}{2} - |y|\right) \right] dy \quad (1)$$

where

$$R_0 = \sqrt{\rho^2 + y^2}, \quad R_1 = \sqrt{\rho^2 + (y - \ell_n/2)^2} \quad \text{and}$$

$$R_2 = \sqrt{\rho^2 + (y + \ell_n/2)^2}$$

The mutual impedance, Z_{21}, can be calculated using (1) when ρ is replaced by d (the spacing between the two wires). The voltage, V_2, of the parasitic wire can be calculated using the current I_1 in (2), and then the phase delay of I_2 can be obtained using (3)

$$V_2 = I_1 Z_{21} \quad (2)$$

$$I_2 = \frac{V_2}{Z_{22}} = \frac{V_1 Z_{21}}{Z_{11} Z_{22}} \quad (3)$$

As d or l_2 increases, the phase delay in the parasitic wire also increases. For instance, for a 0.45-λ parasitic wire, d should be around 0.25λ to obtain ODC (the phase delay is about 160–200°). This demonstrates that ODCs can be realised in single-feed systems by using the main and parasitic wires, provided that appropriately spaced wires of suitable length are used.

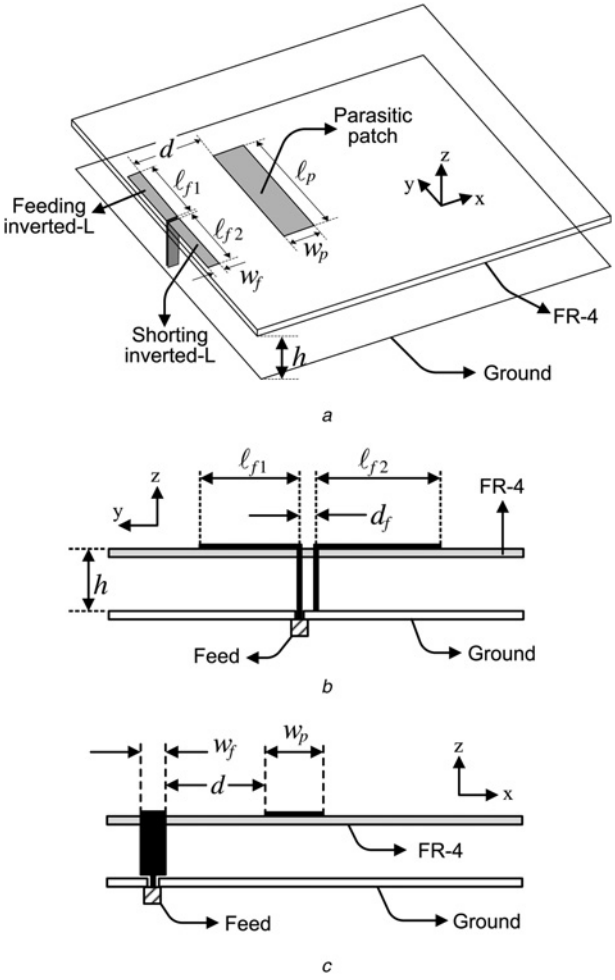

Figure 5 *Proposed antenna structure*

a 3D view
b Side view along *x*-axis
c Side view along *y*-axis

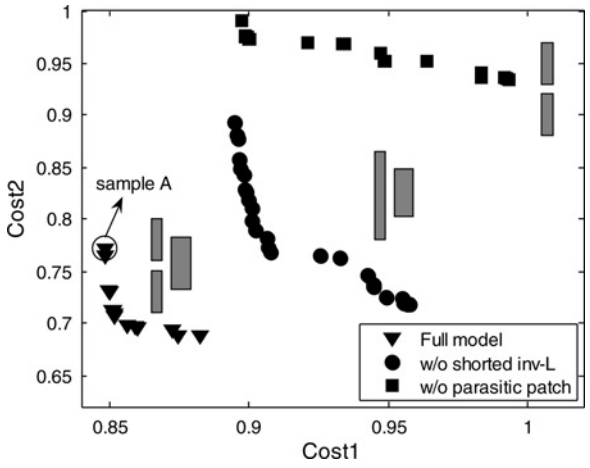

Figure 6 *Optimised results using the Pareto GA*

3 Antenna structure and optimisation

The ODCs described in the previous section were realised as shown in Fig. 5. A symmetrical inverted-L structure ($w_f \times \ell_{f1}$, ℓ_{f2}) was introduced to produce similar currents to a half-wavelength dipole. One end was fed by a coaxial cable and the other was connected to ground. To obtain the ODC, we placed a parasitic patch ($w_p \times \ell_p$) in the vicinity of the symmetric inverted L, where d was the distance between the symmetric inverted L and the parasitic patch. The conducting part of the antenna was printed on a 1.6 mm thick FR-4 substrate. Design parameters, including the height and length of the inverted-L antenna, the size of the parasitic patch and its location were optimised using the PGA in conjunction with the method of moments-based FEKO EM simulator [15, 16]. Fig. 3 shows the approximate design parameters used initially in the PGA process for fast convergence on an optimum solution. The height, h, of the antenna was restricted to less than 50 mm for easy installation on the smart shelf. In the optimisation process, we used two cost functions as follows

$$\text{Cost 1} = 1 - \frac{\int_V |H_z| \mathrm{d}v}{V} \tag{4}$$

$$\text{Cost 2} = \max(|H_z|) - \min(|H_z|) \tag{5}$$

where V is the $30 \times 30 \times 10\ \text{cm}^3$ target volume. Cost 1 is calculated by subtracting the normalised H_z field from 1 and Cost 2 is the deviation of the H_z field over the target surface. The PGA was then used to find solutions that minimised both Cost 1 and Cost 2. The optimised results are plotted as '▼' in Fig. 6. To examine the operating mechanism of each antenna part more closely, we also optimised the design by omitting some antenna parts, such as the shorted inverted L ('•') and the parasitic patch ('■'). The results showed that strong H_z values could not be obtained without the parasitic patch while uniform H_z could not be obtained without the shorted inverted L. Thus, the proposed structure using a symmetrical inverted L and a parasitic patch is necessary to generate strong and uniform H_z over a broad region.

4 Measurement and analysis

To experimentally test our optimised structures, we built and measured a prototype, as shown in Fig. 6, labelled as sample A. The design parameters of the prototype are summarised in Table 1. The surface currents on the symmetric inverted L and the parasitic patch are shown in Fig. 7. As expected, the two currents flowed in opposite directions, and the antenna produced a broad, strong H_z near field. The design parameters, in terms of wavelengths, were as follows: $\ell_{f1} + \ell_{f1} = 0.4\lambda$, $\ell_p = 0.35\lambda$ and $d = 0.12\lambda$. These values are very similar to the results obtained using a simple wire model, as shown in Fig. 3. Fig. 8*a* shows the simulated H_z distribution for the prototype antenna 10 cm above the antenna aperture. The projected antenna structure is plotted as a dashed line in the same figure. The antenna produces H_z values higher than −20 dBA/m in the target reading volume of $30 \times 30 \times 10\ \text{cm}^3$, and H_z distribution is concentrated in this region. We also measured H_z using a small loop probe, and plot the normalised H_z values in Fig. 8*b*. The distribution is in good agreement with the simulation. The measured deviation between the maximum and minimum H_z is less than 12 dB, indicating that the

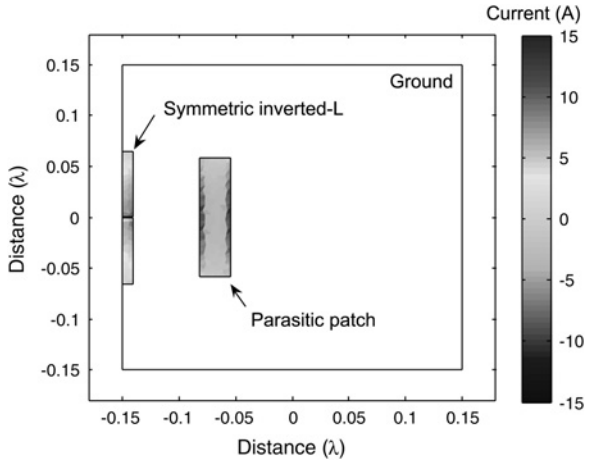

Figure 7 *Current distribution in the prototype*

Table 1 Design parameters of the prototype

Parameters	ℓ_{f1}	ℓ_{f2}	ℓ_p	w_f	w_p	d_f	d	h
length (mm)	64.5	65.6	115.8	9.7	27.3	1	58.8	50

doi: 10.1049/iet-map.2009.0232

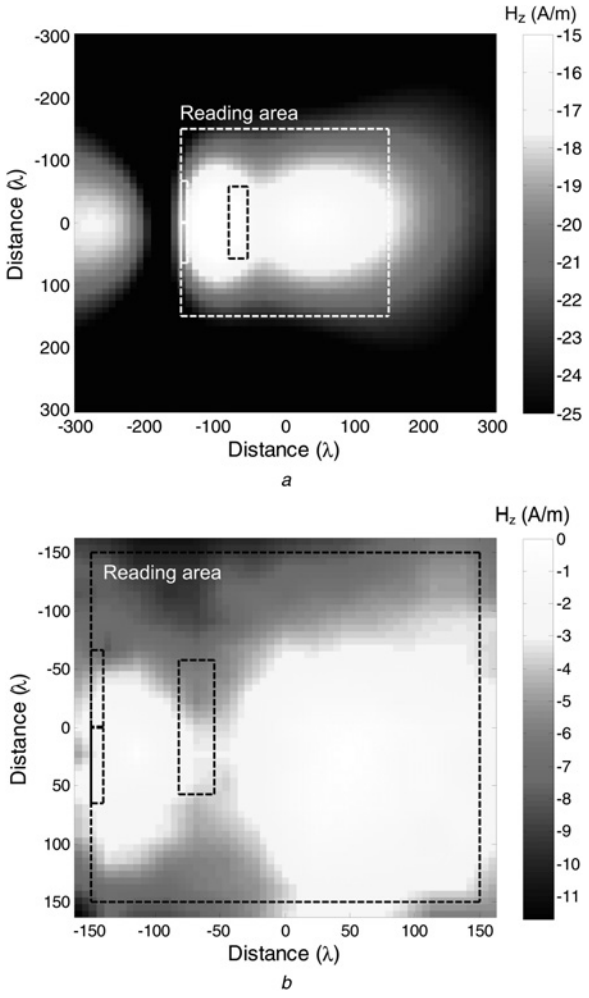

Figure 8 *Near-field H_z distribution of the prototype*

a Simulated H_z near field
b Measured H_z near field (normalised)

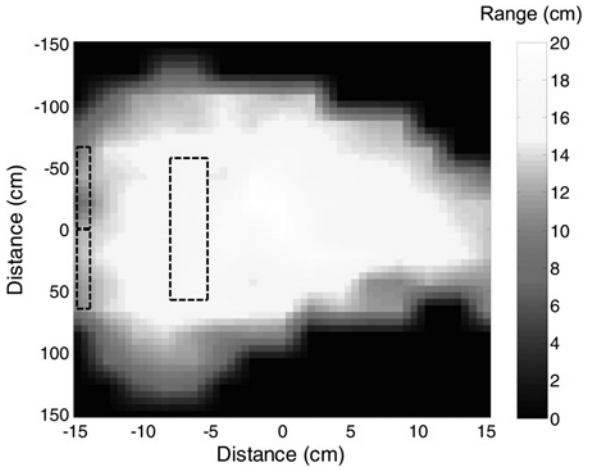

Figure 9 *Maximum reading range using a commercial reader*

proposed antenna achieved stable reading performance in the target region. We measured the reading range using a commercial RFID system, and the results are shown in Fig. 9 [17]. A simple near-field tag antenna with a rectangular loop of $1.0 \times 1.5\ cm^2$ was used with a commercial Gen2 micro-chip [8]. The maximum reading range was 20 cm, the reading area was $634\ cm^2$ and the resulting H_z distribution in the maximum reading range was similar to that shown in Fig. 8.

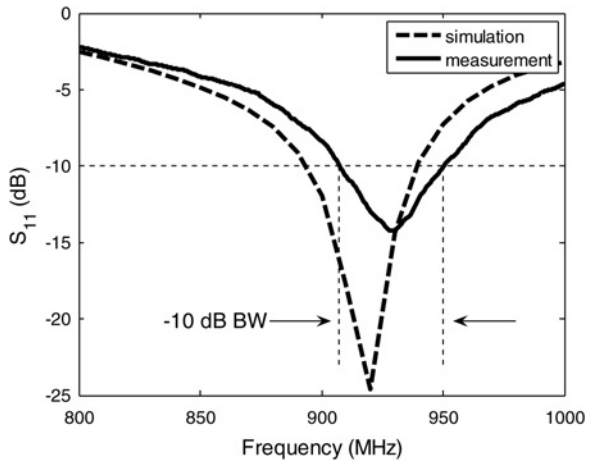

Figure 10 *Return loss of the prototype*

We measured the return loss and radiation pattern to examine the far-field characteristics of the antenna. Fig. 10 shows the simulated and measured reflection coefficients. The resonance frequency for the measurement is slightly shifted by 10 MHz to a higher frequency because of the fabricating error. However, the bandwidth ($S_{11} < -10$ dB) was about 5% (907–950 MHz), and completely covered the RFID bandwidth required in Korea (908.5–914 MHz). The radiation pattern of the proposed antenna is shown in Fig. 11. The measured values agreed well with those of the simulation, and the results show a boresight gain of about 4 dBi, which satisfies the EIRP and ERP regulations in Korea (EIRP < 4 W, ERP < 1.85 W).

A strong advantage of near-field RFID systems is that antenna performance is less affected by nearby dielectric

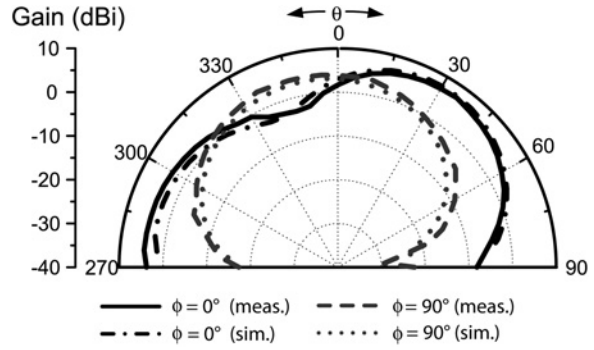

Figure 11 *Radiation pattern of the prototype*

The dash-dotted (simulation) and solid (measured) lines represent the gain in the *H*-plane ($\phi = 0°$), and dotted (simulation) and dashed lines (measurement) represent the gain in the *E*-plane ($\phi = 90°$)

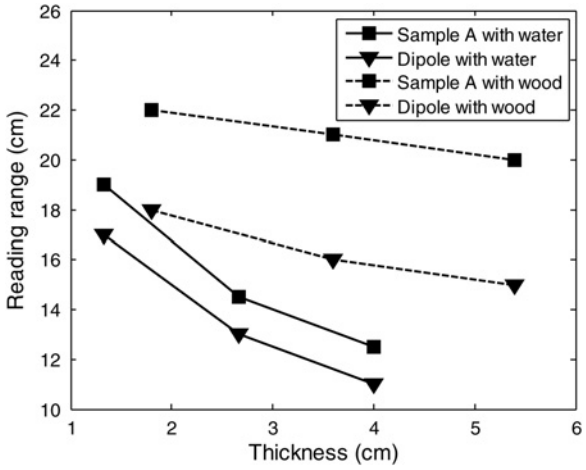

Figure 12 *Variation in the reading range depending on nearby dielectric materials*

materials than are conventional far-field RFID systems. Fig. 12 shows the changes in the reading range when dielectric materials such as wood and water were placed between the reader and the tag. The reading range decreased to 20 cm as the thickness of the wood increased up to 5.4 cm. This result is comparable to the reading range of about 15 cm for the design without a parasitic patch in Fig. 6. The reading range decreased to 12.5 cm when the wood was replaced with water. Under the same conditions, the reading range of the design without a parasitic patch decreased to 11 cm. These results clearly show that the proposed antenna is less affected by nearby dielectric materials than are dipole-type reader antennas.

5 Conclusions

In this paper, we have proposed a novel UHF near-field RFID reader antenna for smart-shelf applications. To obtain a broad, strong near-field H_z, the concept of two closely spaced ODCs was adopted, and this was realised using a symmetric inverted-L structure and a parasitic patch. The design parameters were optimised using PGA. The average H_z of the optimised antenna in the reading volume ($30 \times 30 \times 10$ cm^3) was -20 dBA/m. The proposed antenna covers the required RFID bandwidth and satisfies the EIRP regulations in Korea. The maximum reading range, measured using a small loop with a Gen2 microchip, was 20 cm with a reading area of 634 cm^2. Finally, we examined the effect on our antenna of objects placed in the reading area, and the results show that it is more appropriate for smart-shelf applications than conventional dipole reader antennas.

6 Acknowledgments

This study was supported by the LS Industrial Systems and the IT R&D program of MKE/IITA. [2009-F-042-01, A Study on Mobile Communication System for Next-Generation Vehicles with Internal Antenna Array.]

7 References

[1] AROOR S.R., DEAVOURS D.D.: 'Evaluation of the state of passive UHF RFID: an experimental approach', *IEEE Syst. J.*, 2007, **1**, (2), pp. 168–176

[2] SHAMELI A., SAFARIAN A., ROFOUGARAN A., ROFOUGARAN M., CASTANEDA J., DE FLAVIIS F.D.: 'A UHF near field RFID system with fully integrated transponder', *IEEE Trans. Microw. Theory Tech.*, 2008, **56**, (5), pp. 1267–1277

[3] NIKITIN P.V., RAO K.V.S., LAZAR S.: 'An overview of near field UHF RFID'. IEEE Int. Conf. on RFID, 2007, pp. 176–174

[4] BALANIS C.A.: 'Advanced engineering electromagnetics' (Wiley, New York, 1989)

[5] DIMITRI D.: 'UHF Gen2 for item-level tagging', http://www.impinj.com/files/Impinj_ILT_RFID_World.pdf

[6] RFID and UHF: 'A prescription for RFID success in the pharmaceutical industry', http://www.alientechnology.com/docs/WP_RFID_UHF.pdf

[7] CHOO J., RYOO J., HONG J., PARK K., LEE J.: 'A novel multi-loop tag for near field communication in UHF band'. Proc. Asia-Pacific Microwave Conf., 2007, pp. 1–4

[8] Monza 2, http://www.impinj.com/products/tag-chips.aspx

[9] Higgs 2, http://www.alientechnology.com/tags/rfid_ic.php

[10] KARTHAUS U., FISCHER M.: 'Fully integrated passive UHF RFID transponder IC with 16.7-μW minimum RF input power', *IEEE J. Solid-State Circuits*, 2003, **38**, (10), pp. 1602–1608

[11] KWON I., EO Y., BANG H., *ET AL.*: 'A single-chip CMOS transceiver for UHF mobile RFID reader', *IEEE J. Solid-State Circuits*, 2008, **43**, (3), pp. 729–738

[12] KHANNUR P.B., CHEN X., YAN D.L., *ET AL.*: 'A universal UHF RFID reader IC in 0.18-μm CMOS technology', *IEEE J. Solid-State Circuits*, 2008, **43**, (5), pp. 1146–1155

[13] BALANIS C.A.: 'Antenna theory: analysis and design' (Wiley, New York, 1997)

[14] CPX C.R.: 'Mutual impedance between vertical antennas of unequal heights', *Proc. IRE*, 1947, **35**, (11), pp. 1367–1370

[15] CHOO H., ROGERS R., LING H.: 'Design of electrically small wire antennas using a Pareto genetic algorithm', *IEEE Trans. Antennas Propag.*, 2005, **53**, (3), pp. 1038–1046

[16] FEKO Suite 5.3, http://www.feko.info

[17] CS461 RFID reader, http://www.convergence.com.hk

doi: 10.1049/iet-map.2009.0232